Lithium-Ion Batteries Hot Paper

DOI: 10.1002/anie.201409530

A Hierarchical Tin/Carbon Composite as an Anode for Lithium-Ion Batteries with a Long Cycle Life**

*Xingkang Huang, Shumao Cui, Jingbo Chang, Peter B. Hallac, Christopher R. Fell, Yanting Luo, Bernhard Metz, Junwei Jiang, Patrick T. Hurley, and Junhong Chen**

Abstract: *Tin is a promising anode candidate for next-generation lithium-ion batteries with a high energy density, but suffers from the huge volume change (ca. 260 %) upon lithiation. To address this issue, here we report a new hierarchical tin/carbon composite in which some of the nanosized Sn particles are anchored on the tips of carbon nanotubes (CNTs) that are rooted on the exterior surfaces of micro-sized hollow carbon cubes while other Sn nanoparticles are encapsulated in hollow carbon cubes. Such a hierarchical structure possesses a robust framework with rich voids, which allows Sn to alleviate its mechanical strain without forming cracks and pulverization upon lithiation/de-lithiation. As a result, the Sn/C composite exhibits an excellent cyclic performance, namely, retaining a capacity of 537 mAh g^{-1} for around 1000 cycles without obvious decay at a high current density of 3000 mA g^{-1}.*

Existing commercial graphite anodes are capable of delivering a capacity of approximately 330 mAh g^{-1}, thereby approaching its theoretical capacity (372 mAh g^{-1}). New anodes are required to meet the demands of next-generation lithium-ion batteries (LIBs) for high energy and power densities and a long cycle life. Sn, despite its high costs, is of significant interest and has been investigated extensively because of its high capacity (993.4 mAh g^{-1}; from Sn to $Li_{4.4}Sn$), abundance, and environmentally-friendliness; however, a huge volume change of the Sn anode (ca. 260 %) upon lithiation leads to very poor cyclic performance, inhibiting its practical applications.

[*] Dr. X. K. Huang, Dr. S. M. Cui, Dr. J. B. Chang, Prof. J. H. Chen
Department of Mechanical Engineering
University of Wisconsin-Milwaukee
3200 North Cramer Street, Milwaukee, WI 53211 (USA)
E-mail: jhchen@uwm.edu

P. B. Hallac, C. R. Fell, Y. T. Luo, B. Metz, J. W. Jiang, P. T. Hurley
Global Technology & Innovation, Power Solutions
Johnson Controls
5757 North Green Bay Avenue, Milwaukee, WI 53209 (USA)

[**] Financial support for this work was provided by the U.S. Department of Energy (grant number DE-EE0003208) and Johnson Controls, Inc. The SEM imaging was conducted at the UWM Bioscience Electron Microscope Facility, and TEM analyses were conducted in the UWM Physics HRTEM Laboratory. The authors thank Dr. H. A. Owen, Dr. S. E. Hardcastle, and D. P. Robertson for their technical support with SEM, BET and Raman, and TEM analysis, respectively.

Supporting information for this article is available on the WWW under http://dx.doi.org/10.1002/anie.201409530.

To address this issue, besides employing Sn-based nanocrystals[1,2] and thin films,[3–5] forming SnM (M = Co,[6] Cu,[7] Ni,[8] Mn,[9] Fe,[10] etc.) alloys and Sn/C composites are two effective approaches. Sn/C composites such as Sn@C[11,12] or Sn embedded in C,[13–16] Sn/graphene composites,[17–20] and Sn/carbon nanotube (CNT) composites (including depositing Sn onto CNTs[21,22] or growth of CNTs with Sn as a catalyst[23–26]) have rich pores that can accommodate the volume expansion upon lithiation. CNTs possess excellent electrical conductivity, mechanical strength, and flexibility, and thus is a great matrix for alleviating the mechanical strain of Sn during lithiation/de-lithiation. For previously reported Sn/C composite materials in which Sn is deposited on CNTs, Sn can easily detach from the CNTs because of the weak physical adsorption between them, while for the CNTs grown from Sn catalysts,[23–25] the nanotubes are typically filled with Sn and thus the space is insufficient for the huge volume expansion of Sn during lithiation. Therefore, these Sn/CNTs composites do not exhibit an adequately long cycle life.

Here, we designed and synthesized a new Sn/C hierarchical structure in which some of the nanosized Sn particles are anchored on the tips of CNTs that are rooted on the exterior surfaces of microsized hollow carbon cubes while other Sn nanoparticles are encapsulated in the hollow carbon cubes (Figure 1). Such a hierarchical structure is stable and has rich voids to allow Sn to expand freely, consequently leading to excellent cyclic performance. The carbon in this Sn/C composite not only leads to a good electrical conductivity to achieve an excellent rate capability, but also contributes to the capacity as an active component.

The experimental details are shown in the Supporting Information. In brief, a Na_2CO_3 solution was mixed with a solution containing $SnCl_2$ and $CaCl_2$ (molar ratio Sn/Ca = 1:9). The resulting precipitates were cubic particles with a typical size of 5–10 μm (Figure S1) and consisted of $Sn_6O_4(OH)_4$ and $CaCO_3$ (calcite), as indicated by X-ray diffraction (XRD; Figure S2a). During the deposition of C by chemical vapor deposition (CVD), $CaCO_3$ decomposed to CaO while $Sn_6O_4(OH)_4$ decomposed and was reduced to Sn (Figure S2b). After leaching with dilute HCl, all CaO was removed while only Sn was detected by XRD in the Sn/C composite (Figure S3), which also suggests that C is amorphous in the Sn/C composite.

The scanning electron microscopy (SEM) and transmission electron microscopy (TEM) images shown in Figure 2 suggest the as-prepared Sn/C composite consists of hollow cubes, of which CNTs are rooted on the surface while Sn particles are anchored on the tips of CNTs, consistent with our original design (Figure 1b). The hollow morphology of the

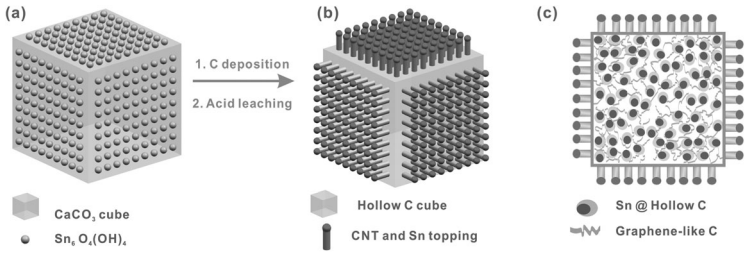

Figure 1. Schematic illustration of the preparation of the Sn/C composite: a) $CaCO_3$ cubes with $Sn_6O_4(OH)_4$ decorated on the surface, b) Sn/C composite, in which Sn particles are anchored on the tips of carbon nanotubes that are rooted on the hollow carbon cubes, and c) cross-section view of the Sn/C composite, showing Sn-encapsulated hollow C and graphene-like C atoms in the hollow C cube.

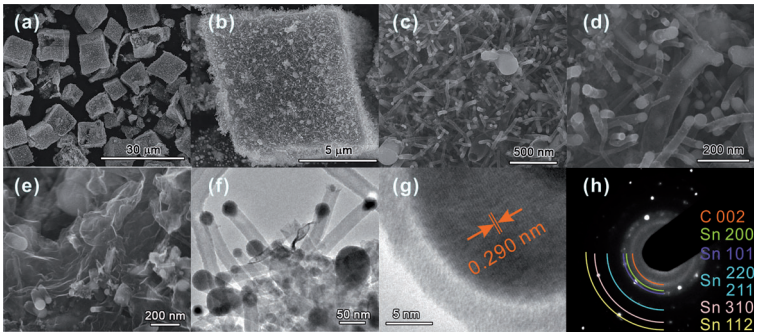

Figure 2. a–e) SEM images of the Sn/C composite: a) overview, b) a single cube, c,d) cube surface, and e) interior view from a broken cube, and f) TEM image, g) HRTEM image, and h) SAED pattern.

Sn/C composite was further confirmed by a cross-sectional observation of an Sn/C composite electrode after cutting by scissors (Figure S4). Energy-dispersive X-ray spectroscopy (EDS) analysis confirms the Sn nanoparticles anchored on the tips of CNTs (Figure S5). Typical diameters of Sn particles range from 20 to 50 nm; the CNTs possess a thick wall (ca. 10 nm; Figure 2 f). The high-resolution TEM (HRTEM) imaging confirms that the nanoparticles on the CNTs are Sn, as the *d*-spacing of 0.290 nm corresponds with the (200) plane of Sn, and the exterior surface of the Sn particle is coated by an amorphous carbon around 4 nm (Figure 2 g). The diffraction ring at 0.36 1 nm on the selected area electron diffraction (SAED) pattern is ascribed to the amorphous carbon in the Sn/C composite (Figure 2 h); this is consistent with the lack of a characteristic peak of C on the XRD pattern (Figure S3b), confirmed by its Raman spectrum showing two broad peaks at 1352 and 1584 cm^{-1}, corresponding with the D and G band of carbon, respectively (Figure S6).

From the broken cubes, we also can observe that some Sn particles are encapsulated inside and accompanied by graphene-like carbon, as suggested by the wrinkles in Figure 2 e. The Sn content in the Sn/C was calculated as 53.2 wt% by thermogravimetric analysis (TGA; Figure S7). X-ray photoelectron spectroscopy (XPS) analysis indicates that the Sn/C atom ratio is 6.7:93.3, corresponding to the 42 wt% of Sn on the surface of the Sn/C composite, suggesting a slightly lower Sn content in the exterior of the Sn/C cube than that in the interior. This is supported by the Sn content of 45 wt% from the XPS analysis after sputtering 12 nm on the surface of the Sn/C composite by Ar ions. Brunauer-Emmett-Teller (BET) analysis indicates the surface area of the as-prepared Sn/C composite is 137.6 $m^2 g^{-1}$; the pore sizes are 27 and 48 nm, calculated from the Barrett-Joyner-Halenda (BJH) desorption and adsorption branches, respectively (Figure S8).

The use of Sn as a catalyst to grow CNTs has been reported with the typical Sn-filled CNTs morphology.[23–25] The formation mechnism for Sn-filled CNTs is believed to follow a "bottom growth" mechanism accompanied by filling CNTs with Sn driven by the capillary force.[27,28] In contrast, Sn nanoparticles anchored on the tip of CNTs in our Sn/C composite have not yet been reported. The formation of the CNTs in our case follows a conventional "tip growth" vapor–liquid–solid (VLS) mechanism,[29] since the Sn catalysts are located on the tip of the CNTs (Figure 2). Because of the low melting point (232 °C) of Sn, Sn in those previous reports[27,28] can be merged to form large liquid particles that act as a source for Sn to fill the CNTs during the growth of CNTs. In our case, however, CaO, decomposed from the $CaCO_3$ precursor, may serve as an isolator that prevents Sn nanoparticles from aggregating and prevents the Sn source from filling the CNTs.

Some CNTs with open tips were observed in the Sn/C composite (Figure 2 c,d). By increasing the Sn content in the Sn/C composite, we can observe more CNTs with open ends, as shown in Figures S9 and S10. The liquid Sn particles were located on the tip of CNTs, but not all of the CNT were growing vertically on the surfaces of the cubes. Along with the CNT growth, some Sn nanoparticles may coalesce with each other to form larger particles, resulting in the open CNTs due to the loss of Sn toppings.

The formation of graphene-like carbon inside the Sn/C cubes (Figure 2 e) was also observed in the case of Sn/Ca = 2:8 during preparation of the precursors (Figure S9). The formation mechanism is likely associated with the decomposition of $CaCO_3$, which resulted in porous CaO while releasing CO_2 gas; the carbon source may enter the cube interiors because of vacuum pressure during synthesis. CaO was then removed by the dilute HCl, leaving the graphene-like carbon. Such carbons are believed to facilitate the electron transfer within Sn particles during charge and discharge processes.

Figure 3 depicts the electrochemical performance of the as-prepared Sn/C composite. The initial discharge (delithiation) capacity at 60 mA g^{-1} is 786.4 mAh g^{-1} (Figure 3 a,b). After activation for the initial two cycles, the anode was cycled at 600 mA g^{-1}, exhibiting capacities of 596.2 and 626.4 mAh g^{-1} for the 4th and 200th cycles, respectively (Figure 3 b). Figure 3 c,d shows the rate capability of the Sn/C composite; the capacities at 60, 120, 300, 600, 1200, 3000, and 6000 mA g^{-1} are 798.2, 751.8, 670.8, 610.8, 549.7, 464.9, and 341.6 mA g^{-1}, respectively. After the rate capability test, the

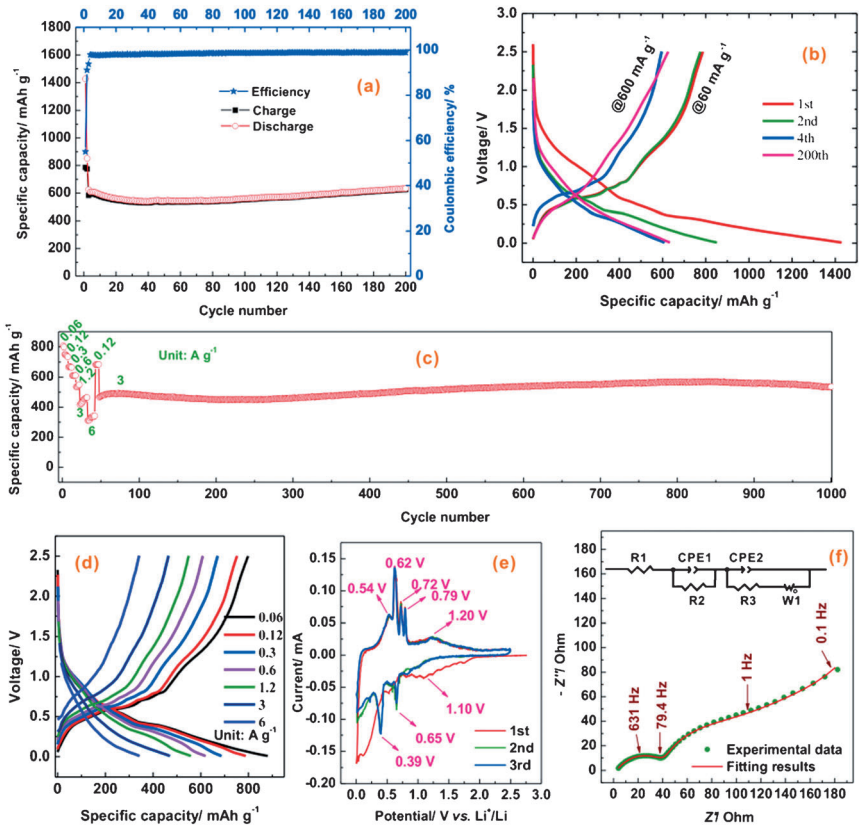

Figure 3. Electrochemical performance of the Sn/C composite. a) cyclic performance at 600 mA g^{-1} after activation at 60 mA g^{-1} for the initial two cycles, b) charge/discharge curves, c,d) rate capability, e) cyclic voltammetry, and f) EIS plot; the inset shows the two-time constant equivalent circuit for fitting the EIS plot.

anode was cycled at 3000 mA g^{-1} for an additional 953 cycles, exhibiting 536.5 mAh g^{-1} at the 1000th cycle. The excellent cyclic performance of such a Sn/C composite is associated with its stable hierarchical structure, whereas Sn particles are encapsulated in the hollow C cubes or anchored on the tips of CNTs that are rooted on the surfaces of C cubes. In contrast, an Sn encapsulated C composite without formation of CNTs exhibited much poorer cyclic performance (Figure S11) than the Sn-anchored CNTs rooted on C. In addition, if we double or triple the Sn content in the composite, the Sn toppings will have a greater chance to collide with each other and form large particles (Figures S9, S10); the resulting Sn/C composites show much poorer cyclic performance (Figure S12). These results confirmed the high dependence of the cyclic performance of the Sn/C composite on our designed hierarchical structure, in which the rich voids allow Sn to release the strain upon lithiation, without resulting in severe cracks in the anode, as evidenced by the SEM and TEM images of the Sn/C composite anode after cycling (Figures S13–S15).

Until now, there are only a few reports on Sn-based anodes capable of cycling up to 1000 cycles. For example, an Sn nanoparticle-decorated, three-dimensional, foothill-like graphene was reported as a thin-film anode with 4000 cycles; the anode showed a capacity of 1349 mAh g^{-1} at 879 mA g^{-1} while decaying to 460 mAh g^{-1} (namely, 34.1 % retained) within a dozen initial cycles and then remaining stable until 4000 cycles.[30] Recently, Qin et al.[31] prepared Sn nanoparticles anchored on interconnected C cubes by using citric acid, $SnCl_2{\cdot}2H_2O$, and NaCl through a freeze-drying technology and heat treatment in H_2; the Sn/C anode showed 682 mAh g^{-1} at a cutoff range between 0.005 and 3 V at 2 A g^{-1} and retained approximately 96.3 % capacity after 1000 cycles. Compared with these excellent results, our Sn/C shows even more superior electrochemical performance, delivering about 537 mAh g^{-1} at 3000 mA g^{-1} for about 1000 cycles without obvious decay, and with an excellent rate capability; for example, our Sn/C exhibited 341.6 mAh g^{-1} at 6000 mA g^{-1}, which is 43 % of the capacity (798.2 mAh g^{-1}) obtained at 60 mA g^{-1}.

Figure 3e exhibits the cyclic voltammetry (CV) of the Sn/C composite. During the first cathodic scan, the irreversible peak at about 1.10 V is associated with solid electrolyte interphase (SEI) layer formation and reduction of SnO_x on the surface of Sn. Sn is well-known to oxidize easily on the surface; XPS characterization confirms that Sn surfaces were covered by SnO_x (Figure S16). After activation during the first cathodic scan, the well-overlapped peaks on the subsequent CV curves confirm an excellent cyclic performance of the Sn/C composite. The anodic scan on the CV curves of our Sn/C composite shows four peaks related to Sn at 0.54, 0.62, 0.72, and 0.79 V corresponding with $Li_{22}Sn_5$ to Li_7Sn_3, LiSn, Li_2Sn_5, and Sn, respectively;[32] in contrast, the peak at 1.20 V is ascribed to the conversion of LiC_x to C, because this peak is unavailable for a pure Sn anode,[3] and low C-content Sn/C composite anode.[33]

The initial discharge capacity of our Sn/C composite is 768.4 mAh g^{-1} (Figure 3a), beyond the maximum capacity of 501.9 mAh g^{-1} that Sn in the Sn/C composite can contribute to because the Sn content in the composite is 53.2 wt %. C in the composite thus contributed 266.5 mAh g^{-1}, corresponding with 569.4 mAh $(g(C))^{-1}$. Graphene has a theoretical capacity of 774 mAh g^{-1},[27] while CNTs were reported to have a capacity of 782.4 mAh g^{-1}.[34] In fact, a significant contribution from C has been previously reported for Sn/C composites in the literature.[5,14,27,35] By comparing the discharge curves of Sn/C composites with various Sn contents, we also can confirm the contribution from carbon. As shown in Figure S17, the major difference between the two Sn/C composites is located above 1.0 V in their discharge curves; the higher C content results in greater capacity located above 1.0 V, consistent with the anodic peak at 1.20 V in the CV curves (Figure 3e); the capacity above 1.0 V is negligible for a pure Sn anode.[3] The peak at 1.2 V is absent on the dQ/dV plot of the Sn/C composite in the case Sn/Ca is 3:7 (Fig-

ure S18) because of its low C content (11.5 wt.%; Table S1). Meanwhile, graphene was reported to deliver a capacity of 540 mAh g^{-1} with around only 100 mAh g^{-1} located below 1.0 V.[36] The capacity located above 1.0 V of the Sn/C composite (53.2 wt.% Sn; Sn/Ca = 1:9 in the precursor) is determined to be 299 mAh g^{-1}, close to 266.5 mAh g^{-1}, the contributed value from C, if assuming the contribution from Sn is 943.4 mAh g^{-1}.

The electrochemical impedance spectroscopy (EIS; Figure 3 f) measurement indicates that the Nyquist plot of the Sn/C composite consists of two semi-circles at high and moderate frequencies, and an inclined line at a low frequency, corresponding with the resistances of SEI layer, charge transfer, and lithium ion diffusion in the solid phase, respectively. By fitting the Nyquist plot with Zview software by using a two-time constant equivalent (inset in Figure 3 f), the Ohmic, SEI layer, charge transfer, and Li^+ diffusion resistances were determined to be 2.5, 43.1, 29.9, and 13.3 Ohm, respectively. The small resistances agree well with the excellent rate capability of the Sn/C composite (Figure 3 d).

In conclusion, we designed and synthesized a novel hierarchical Sn/C composite, in which Sn nanoparticles are either encapsulated in hollow C cubes or anchored on the tip of CNTs that rooted on the surfaces of hollow C cubes. Such a composite offers rich voids and a very stable structure, which allows Sn to have enough spaces to accommodate the large volume change upon lithiation. The Sn/C composite delivered a capacity of 786.4 mAh g^{-1} at the current density of 60 mAh g^{-1} and no capacity degradation was observed for 200 cycles when cycling at 600 mA g^{-1}. Furthermore, the Sn/C composite performed at 3000 mA g^{-1} for around 1000 cycles while showing a capacity of 537 mAh g^{-1} without obvious decay. Therefore, such a hierarchical Sn/C composite is a very promising anode material for LIBs.

Received: September 26, 2014
Published online: December 10, 2014

Keywords: carbon nanotubes · electrochemistry · lithium-ion batteries · nanoparticles · tin anode

[1] L. P. Xu, C. Kim, A. K. Shukla, A. G. Dong, T. M. Mattox, D. J. Milliron, J. Cabana, *Nano Lett.* **2013**, *13*, 1800 – 1805.
[2] Y. Yu, L. Gu, X. Y. Lang, C. B. Zhu, T. Fujita, M. W. Chen, J. Maier, *Adv. Mater.* **2011**, *23*, 2443 – 2447.
[3] K. Ui, S. Kikuchi, Y. Kadoma, N. Kumagai, S. Ito, *J. Power Sources* **2009**, *189*, 224 – 229.
[4] A. Marcinek, L. J. Hardwick, T. J. Richardson, X. Song, R. Kostecki, *J. Power Sources* **2007**, *173*, 965 – 971.
[5] W. Li, R. Yang, J. Zheng, X. G. Li, *Nano Energy* **2013**, *2*, 1314 – 1321.
[6] Y. Gu, F. D. Wu, Y. Wang, *Adv. Funct. Mater.* **2013**, *23*, 893 – 899.
[7] C. Arbizzani, M. Lazzari, M. Mastragostino, *J. Electrochem. Soc.* **2005**, *152*, A289 – A294.
[8] K. K. D. Ehinon, S. Naille, R. Dedryvere, P. E. Lippens, J. C. Jumas, D. Gonbeau, *Chem. Mater.* **2008**, *20*, 5388 – 5398.
[9] L. Y. Beaulieu, J. R. Dahn, *J. Electrochem. Soc.* **2000**, *147*, 3237 – 3241.
[10] X. L. Wang, M. Feygenson, H. Y. Chen, C. H. Lin, W. Ku, J. M. Bai, M. C. Aronson, T. A. Tyson, W. Q. Han, *J. Am. Chem. Soc.* **2011**, *133*, 11213 – 11219.
[11] Y. S. Jung, K. T. Lee, J. H. Ryu, D. Im, S. M. Oh, *J. Electrochem. Soc.* **2005**, *152*, A1452 – A1457.
[12] K. T. Lee, Y. S. Jung, S. M. Oh, *J. Am. Chem. Soc.* **2003**, *125*, 5652 – 5653.
[13] Z. Q. Zhu, S. W. Wang, J. Du, Q. Jin, T. R. Zhang, F. Y. Cheng, J. Chen, *Nano Lett.* **2014**, *14*, 153 – 157.
[14] J. C. Guo, Z. C. Yang, L. A. Archer, *J. Mater. Chem. A* **2013**, *1*, 8710 – 8715.
[15] Z. Tan, Z. H. Sun, H. H. Wang, Q. Guo, D. S. Su, *J. Mater. Chem. A* **2013**, *1*, 9462 – 9468.
[16] Y. C. Qiu, K. Y. Yan, S. H. Yang, *Chem. Commun.* **2010**, *46*, 8359 – 8361.
[17] S. Z. Liang, X. F. Zhu, P. C. Lian, W. S. Yang, H. H. Wang, *J. Solid State Chem.* **2011**, *184*, 1400 – 1404.
[18] G. X. Wang, B. Wang, X. L. Wang, J. Park, S. X. Dou, H. Ahn, K. Kim, *J. Mater. Chem.* **2009**, *19*, 8378 – 8384.
[19] B. Luo, B. Wang, X. L. Li, Y. Y. Jia, M. H. Liang, L. J. Zhi, *Adv. Mater.* **2012**, *24*, 3538 – 3543.
[20] C. Nithya, S. Gopukumar, *ChemSusChem* **2013**, *6*, 898 – 904.
[21] Z. P. Guo, Z. W. Zhao, H. K. Liu, S. X. Dou, *Carbon* **2005**, *43*, 1392 – 1399.
[22] M. H. Wu, C. Wang, J. Chen, F. Q. Wang, B. L. Yi, *Ionics* **2013**, *19*, 1341 – 1347.
[23] K. C. Hsu, C. E. Liu, P. C. Chen, C. Y. Lee, H. T. Chiu, *J. Mater. Chem.* **2012**, *22*, 21533 – 21539.
[24] Y. Wang, M. Wu, Z. Jiao, J. Y. Lee, *Chem. Mater.* **2009**, *21*, 3210 – 3215.
[25] W. Ni, Y. B. Wang, R. Xu, *Part. Part. Syst. Charact.* **2013**, *30*, 873 – 880.
[26] X. Y. Hou, H. Jiang, Y. J. Hu, Y. F. Li, J. C. Huo, C. Z. Li, *ACS Appl. Mater. Interfaces* **2013**, *5*, 6672 – 6677.
[27] Y. Q. Zou, Y. Wang, *ACS Nano* **2011**, *5*, 8108 – 8114.
[28] D. Deng, J. Y. Lee, *Angew. Chem. Int. Ed.* **2009**, *48*, 1660 – 1663; *Angew. Chem.* **2009**, *121*, 1688 – 1691.
[29] M. Kumar, Y. Ando, *J. Nanosci. Nanotechnol.* **2010**, *10*, 3739 – 3758.
[30] C. D. Wang, Y. Li, Y. S. Chui, Q. H. Wu, X. F. Chen, W. J. Zhang, *Nanoscale* **2013**, *5*, 10599 – 10604.
[31] J. Qin, C. N. He, N. Q. Zhao, Z. Y. Wang, C. S. Shi, E. Z. Liu, J. J. Li, *ACS Nano* **2014**, *8*, 1728 – 1738.
[32] M. Winter, J. O. Besenhard, *Electrochim. Acta* **1999**, *45*, 31 – 50.
[33] M. Uysal, T. Cetinkaya, A. Alp, H. Akbulut, *Appl. Surf. Sci.* **2014**, *290*, 6 – 12.
[34] D. T. Welna, L. T. Qu, B. E. Taylor, L. M. Dai, M. F. Durstock, *J. Power Sources* **2011**, *196*, 1455 – 1460.
[35] N. A. Kaskhedikar, J. Maier, *Adv. Mater.* **2009**, *21*, 2664 – 2680.
[36] E. Yoo, J. Kim, E. Hosono, H. Zhou, T. Kudo, I. Honma, *Nano Lett.* **2008**, *8*, 2277 – 2282.

